Chemical Science

ROYAL SOCIETY OF CHEMISTRY

EDGE ARTICLE

View Article Online
View Journal

Check for updates

Cite this: DOI: 10.1039/d5sc02644j

All publication charges for this article have been paid for by the Royal Society of Chemistry

Open Access Article. Published on 19 May 2025. Downloaded on 6/2/2025 5:20:26 PM. This article is licensed under a Creative Commons Attribution 3.0 Unported Licence.

# Isolable monoatomic monovalent bismuth complexes with a redox non-innocent bis-silylenyl carborane ligand†

Jian Xu,[a] Shenglai Yao,[a] Verònica Postils,[b] Eduard Matito,[cd] Christian Lorent[e] and Matthias Driess*[a]

Received 9th April 2025
Accepted 16th May 2025

DOI: 10.1039/d5sc02644j

rsc.li/chemical-science

Utilizing the chelating bis(silylenyl)carborane [$Si^{II}$(*closo*-CB)$Si^{II}$] (**A**, $Si^{II}$ = PhC(N*t*Bu)$_2$Si, CB = *o*-$C_2B_{10}H_{10}$) ligand, a series of unprecedented bis(silylene)-stabilized monovalent bismuth complexes {[$Si^{II}$(*closo*-CB)$Si^{II}$]Bi}X (X = I, **1a**; X = OTf, **1b**), {[$Si^{II}$(*nido*-CB)$Si^{II}$]Bi} (**2**) and ({[$Si^{II}$(*nido*-CB)$Si^{II}$]Bi}K(thf)$_2$)$_2$ ([**3**K(thf)$_2$]$_2$) were synthesized, isolated and characterized. The electronic structures of the bismuth complexes are significantly influenced by the redox-active nature of the CB scaffold. Remarkably, a one-electron injection to **1b** with $KC_8$ does not furnish a $Bi^0$ complex but reduction of the CB backbone giving rise to the neutral $Bi^I$ radical complex **2**. Notably, compound **1b** can also undergo a two-electron reduction with two molar equiv. of potassium naphthalenide, resulting in the formation of the diamagnetic $Bi^I$ anion complex **3** as a dimer bridged *via* two K(thf)$_2$ cations. Density functional theory calculations reveal that upon reduction from **1a** to **2**, and **2** to **3**, the added electron predominantly localizes within the carborane cage, with a marked preference for the carbon atoms, ruling out that these species exhibit characteristics of a molecular bismuth(0) electride.

## Introduction

Bismuth, known since ancient times, is the heaviest stable element in the periodic table, possessing an extraordinarily long half-life of $1.9 \times 10^{19}$ years.[1,2] Despite its inherent stability, bismuth has been widely utilized in diverse research fields, including medical science, physical and materials sciences, and applied chemistry.[3–7] In recent years, significant progress has been made in the study of low-valent bismuth compounds,[8–10] highlighting their multiple accessible oxidation states and redox-active nature. These characteristics enable bismuth to participate in a variety of chemical transformations, presenting exciting opportunities for innovative catalytic applications.[11–13] Furthermore, bismuth has emerged as a promising central ion in single-molecule magnets (SMMs) due to its strong spin–orbit coupling and stable multivalent states.[14–16]

Monoatomic zero-valent complexes of Group 14 elements, known as tetrylones, adopt the general formula L: → $E^0$ ←: L (E = C, Si, Ge, Sn, Pb; L = Lewis donor ligands).[17–21] Mono-valent cationic bismuth species can be regarded as the heaviest isoelectronic analogs of tetrylones, that is plumbylones, possessing two lone pairs on the central atom.[22,23] The first cationic $Bi^I$ compound (**I**, Fig. 1)[24] was synthesized by reducing $BiCl_3$ in the presence of cyclic alkyl(amino)carbenes (cAACs). Subsequently, the bis(silylene)-supported $Bi^I$ cation complex [{$Si^{II}$(TBD)$Si^{II}$}$Bi^I$][$BAr^F{}_4$] **II** (ref. 25) ($Si^{II}$ = PhC(N*t*Bu)$_2$Si, TBD = 1,8,10,9-triazaboradecalin, $Ar^F$ = 3,5-(CF$_3$)$_2$-C$_6$H$_3$) was prepared

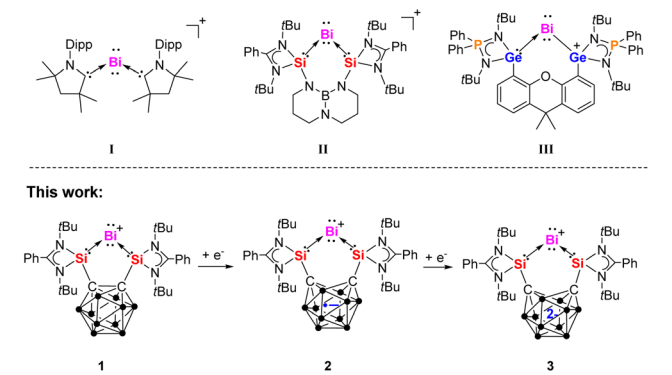


Fig. 1 Known examples of cationic $Bi^I$ complexes **I**–**III** and the $Bi^I$ species **1**–**3** of this work bearing a redox non-innocent carborane cage.

[a]*Metalorganic and Inorganic Materials, Department of Chemistry, Technische Universität Berlin, 10623 Berlin, Germany. E-mail: matthias.driess@tu-berlin.de*
[b]*Theoretical Chemistry Group, Molecular Chemistry, Materials and Catalysis Division (MOST), Institute of Condensed Matter and Nanosciences, Université Catholique de Louvain, Place Louis Pasteur 1, B-1348 Louvain-la-Neuve, Belgium*
[c]*Donostia International Physics Center (DIPC), 20018 Donostia, Euskadi, Spain*
[d]*Ikerbasque Foundation for Science, Plaza Euskadi 5, 48009 Bilbao, Euskadi, Spain*
[e]*Physical and Biophysical Chemistry, Department of Chemistry, Technische Universität Berlin, 10623 Berlin, Germany*

† Electronic supplementary information (ESI) available. CCDC 2428091–2428095. For ESI and crystallographic data in CIF or other electronic format see DOI: https://doi.org/10.1039/d5sc02644j

© 2025 The Author(s). Published by the Royal Society of Chemistry

Open Access Article. Published on 19 May 2025. Downloaded on 6/2/2025 5:20:26 PM. This article is licensed under a Creative Commons Attribution 3.0 Unported Licence.

through a one-pot reaction between the bis(silylene) {$Si^{II}$(TBD)$Si^{II}$} ligand and [IPr → $BiBr_3$] (IPr = 1,3-bis(2,6-diisopropylphenyl)-imidazole-2-ylidene), followed by treatment with $Na[BAr^F{}_4]$ in THF at −30 °C and reduction with two molar equiv. of potassium graphite ($KC_8$). Recently, our group reported the bis(germylene)-supported cationic $Bi^I$ complex **III**.[26] Due to the redox non-innocent nature of the germylene moieties, the positive charge of the $Bi^I$ cation migrates to one of the Ge atoms within the bis(germylene) ligand, resulting in the chelating germylium–germylene $Bi^I$ complex **III**.

In recent years, our group has successfully designed and synthesized several chelating bis(NHSi) ligands (NHSi = *N*-heterocyclic silylene) featuring electronically and geometrically diverse spacers.[27] These bis(NHSi) ligands have facilitated the isolation of various low-valent main-group compounds, including zero-valent group 14 and mono-valent group 15 complexes, which exhibit fascinating electronic structures and unique chemical reactivities.[28–35] The bis(silylenyl)-*o*-carborane ligand [$Si^{II}$(*closo*-CB)$Si^{II}$] (**A**, $Si^{II}$ = PhC(N*t*Bu)$_2$Si, CB = *o*-$C_2B_{10}H_{10}$)[36] (Scheme 1), featuring a relatively short $Si^{II}\cdots Si^{II}$ distance of approximately 3.3 Å, was first reported by our group in 2016. The latter ligand acts as a strong chelating Lewis donor due to the silylene moieties and exhibits interesting redox non-innocence attributed to the carborane spacer. These properties have proven effective in stabilizing monoatomic $Si^0$ and $Ge^0$ complexes[33,34] as well as containing the isoelectronic $N^I$ cation.[35] Herein, we report the synthesis and characterization of the $Bi^I$ cation complexes {[$Si^{II}$(*closo*-CB)$Si^{II}$]Bi}X (X = I, **1a**; X = OTf, **1b**) supported by the bis(silylenyl)-*o*-carborane **A**. Strikingly, the one-electron and two-electron reductions of **1b** using $KC_8$ and $KC_{10}H_8$, respectively, yield no $Bi^0$ species but the neutral and anionic $Bi^I$ complexes {[$Si^{II}$(*nido*-CB)$Si^{II}$]Bi} **2** and ({[$Si^{II}$(*nido*-CB)$Si^{II}$]Bi}K(thf)$_2$)$_2$ ([**3**K(thf)$_2$]$_2$), both featuring a *nido*-$C_2B_{10}$ core, yet in different reduced states. The electronic structures of this series of $Bi^I$ complexes are further elucidated through Density Functional Theory (DFT) calculations.

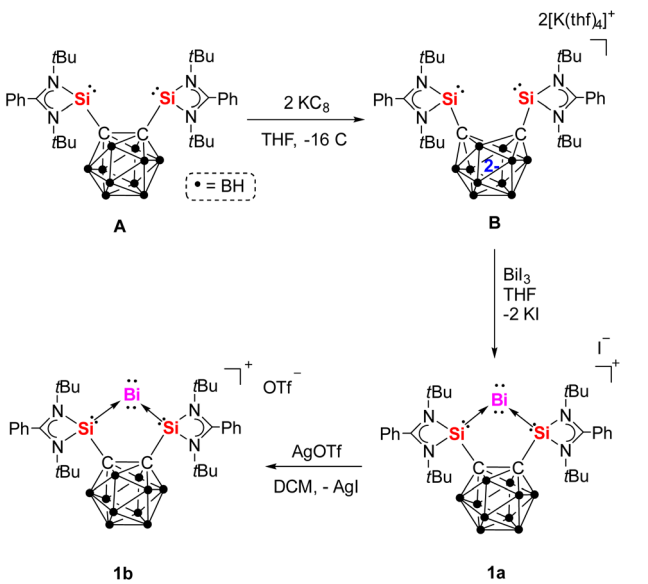


Scheme 1 Synthesis of $Bi^I$ cation complexes **1a** and **1b** from bis(silylenyl)-*o*-carborane **A**.

## Results and discussion

### Synthesis of bis(silylene)-stabilized mono-valent single atom bismuth complexes

The dipotassium bis(silylenyl)-*nido*-dicarboranate precursor [{$Si^{II}$(*nido*-CB)$Si^{II}$}][$K_2$(thf)$_4$] (**B**),[33] generated *in situ* from bis(silylenyl)-*o*-carborane (**A**) and two molar equivalents of $KC_8$ in THF (Scheme 1), reacts with one equiv. of $BiI_3$ at −30 °C to afford the $Bi^I$ cation complex **1a**. After workup, the desired $Bi^I$ complex {[$Si^{II}$(*closo*-CB)$Si^{II}$]Bi}I (**1a**) was isolated as brown-yellow needle-shaped crystals in 57% yield. Subsequent treatment of **1a** with one equiv. of AgOTf in dichloromethane (DCM) results in the replacement of the iodide counterion by $OTf^-$, yielding the {[$Si^{II}$(*closo*-CB)$Si^{II}$]Bi}OTf complex **1b** as an orange powder in 77% yield. The $^{29}Si\{^1H\}$ NMR spectra of **1a** and **1b** show singlets at $\delta$ = 68.7 and 66.9 ppm, respectively, both exhibiting significant downfield shifts relative to **A** ($\delta$ = 18.9 ppm).[28]

The molecular structures of **1a** and **1b** were determined by single-crystal X-ray diffraction (scXRD) analysis. Both exhibit a discrete ionic structure with a similar five-membered $C_2Si_2Bi$ ring in the cation, where the central $Bi^I$ site is coordinated to two silicon atoms. The Si–Bi bond lengths range from 2.5774(6) to 2.5958(9) Å (Fig. 2), similar to those in the [{$Si^{II}$(TBD)$Si^{II}$}$Bi^I$][$BAr^F{}_4$] complex **II** (Fig. 1, 2.557(1) and 2.561(8) Å).[25] The Si–C bond lengths span from 1.923(2) to 1.937(4) Å, while the $C_1$–$C_2$ distances in **1a** and **1b** [1.691(5) and 1.692(3) Å] are very close to that in **A** (1.71 Å).[36] Notably, the $Si_1$–$Bi_1$–$Si_2$ angles of 79.28(3)° and 79.486(18)° in **1a** and **1b** are slightly more acute than in complex **II** [82.10(3)°].[25]

Notably, the cyclic voltammogram (CV) of **1b** exhibits two quasi-reversible reduction processes at $E_{1/2}$ = −1.36 V and −1.68 V *vs.* $Fc/Fc^+$ (see ESI Fig. S11†). This prompted us to explore its chemical reduction. Upon mixing **1b** with one equivalent of $KC_8$ in THF at −30 °C, a deep-red solution formed, from which complex **2** was isolated in 43% yield (Scheme 2).

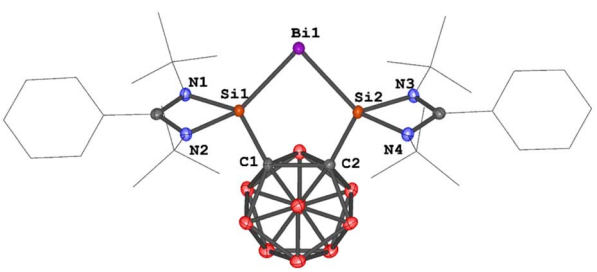


Fig. 2 Molecular structures of the cations in **1a** and **1b**. Thermal ellipsoids are drawn at the 50% probability level. H atoms, anionic moieties and solvent molecules are omitted for clarity. Selected bond lengths (Å) and angles (deg.): **1a**: $Bi_1$–$Si_2$ 2.5958(9), $Bi_1$–$Si_1$ 2.5940(10), $C_2$–$C_1$ 1.691(5), $Si_2$–$C_2$ 1.937(4), $Si_1$–$C_1$ 1.937(4), $Si_1$–$Bi_1$–$Si_2$ 79.28(3), $C_1$–$Si_1$–$Bi_1$ 115.14(11), $C_2$–$Si_2$–$Bi_1$ 115.65(11). **1b**: $Bi_1$–$Si_2$ 2.5774(6), $Bi_1$–$Si_1$ 2.5931(6), $C_2$–$C_1$ 1.692(3), $Si_1$–$C_1$ 1.923(2), $Si_2$–$C_2$ 1.925(2), $Si_1$–$Bi_1$–$Si_2$ 79.486(18), $C_1$–$Si_1$–$Bi_1$ 115.25(7), $C_2$–$Si_2$–$Bi_1$ 115.53(7).


© 2025 The Author(s). Published by the Royal Society of Chemistry

Open Access Article. Published on 19 May 2025. Downloaded on 6/2/2025 5:20:26 PM.
This article is licensed under a Creative Commons Attribution 3.0 Unported Licence.

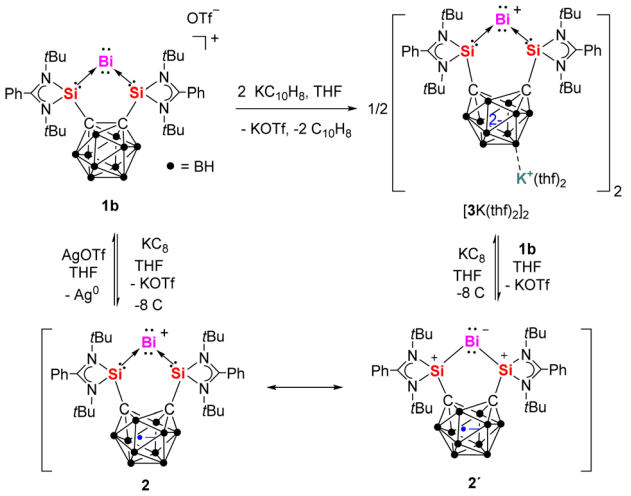


Scheme 2 Reversible redox reactions between **1b**, **2** (with its resonance structure **2′**) and $[\mathbf{3}K(thf)_2]_2$.

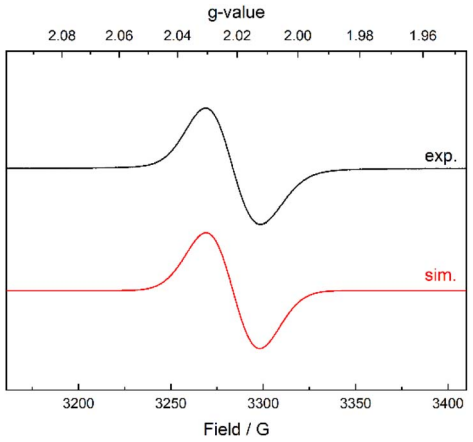


Fig. 4 EPR spectrum of compound **2** in THF (top) recorded at 293 K and the corresponding simulation (bottom). The *g*-value of the radical species is 2.023 and the line width 29.1 G.

An scXRD analysis revealed that compound **2** crystallizes as a neutral $Bi^{I}$ radical complex in the orthorhombic space group *Cmcm*. Its molecular structure features an open-cage *nido*-carborane backbone with a C⋯C distance of 2.268 Å (Fig. 3). The $Si_1$–$Bi_1$ bond length of 2.576(2) Å is comparable to those in complexes **1a** and **1b** (2.5774(6)–2.5958(9) Å). However, the $Si_1$–$C_1$ bond in complex **2** (1.851(8) Å) is significantly shorter than in **1a** and **1b** (1.923(2)–1.937(4) Å). Notably, the $Si_1$–$Bi_1$–$Si_{1a}$ bond angle in complex **2** (86.25(8)°) is substantially larger than in **1a** and **1b** (∼79°), likely due to the open-cage nature of the carborane backbone.

Compound **2** is paramagnetic and shows broad resonance peaks in solution $^{1}$H NMR spectra at room temperature (see ESI, Fig. S13†). Accordingly, the electron paramagnetic resonance (EPR) spectrum of **2** recorded at room temperature in THF (Fig. 4) exhibits an isotropic signal at $g = 2.0229$ (line width = 29.1 G). Though the band shape is very similar to the one of the known $N^{I}$ anionic carborane radical $\{[Si^{II}(nido\text{-}CB)Si^{II}]N^{I}\}$,[35] the *g*-value is slightly higher than those typical for such organic radicals. Magnetic interactions with the nearby very heavy Bi nucleus could be the origin. An unpaired spin located at the Bi itself can be excluded based on the EPR spectrum at 10 K (see ESI, Fig. S14†), which lacks the characteristic broad and multiline features of a Bi-centred radical ($Bi^{0}$).[26] Overall, the observations indicate that the unpaired electron is localized in the carborane cage (see electronic structure discussion below).

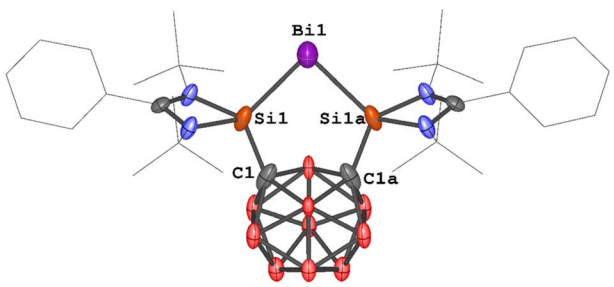


Fig. 3 Molecular structure of **2**. Thermal ellipsoids are drawn at the 50% probability level. H atoms and solvent molecules are omitted for clarity. Selected bond lengths (Å) and angles (deg.): $C_1$–$Si_1$ 1.851(8), $Si_1$–$Bi_1$ 2.576(2), $C_1$⋯$C_{1a}$ 2.268, $Si_1$–$Bi_1$–$Si_{1a}$ 86.25(8), $C_1$–$Si_1$–$Bi_1$ 117.1(3).

To investigate the reversibility of the latter one-electron reduction, compound **2** was allowed to react with equimolar amount of AgOTf in THF at room temperature. Indeed, compound **1b** was quantitatively regenerated after stirring for 10 minutes (Scheme 2). Given the carborane moiety of bis(NHSi) can store one or two electrons, we further explored the two-electron reduction of **1b**. The reaction of **1b** with two molar equiv. of potassium naphthalenide ($KC_{10}H_8$) in THF at −30 °C yielded complex $(\{[Si^{II}(nido\text{-}CB)Si^{II}]Bi\}K(thf)_2)_2$ ($[\mathbf{3}K(thf)_2]_2$) as a brown powder in 51% yield (Scheme 2). Its $^{1}$H NMR spectrum in THF-$d_8$ displays one singlet at $\delta = 1.29$ ppm for the *tert*-butyl groups, while the $^{29}Si\{^{1}H\}$ NMR spectrum exhibits a singlet at $\delta = 51.8$ ppm, significantly upfield-shifted compared to **1a** ($\delta = 68.7$ ppm) and **1b** ($\delta = 66.9$ ppm).

An scXRD analysis reveals that ($[\mathbf{3}K(thf)_2]_2$) adopts a dimeric structure in the solid state, with two $[K(thf)_2]^{+}$ moieties acting as linkers *via* B–H⋯K⋯H–B interactions (Fig. 5). The Si–Bi bond lengths in ($[\mathbf{3}K(thf)_2]_2$) (2.6266(13) and 2.6138(13) Å) are slightly longer than those in **1a** and **1b** (2.5774(6)–2.5958(9) Å) and in **2** (2.576(2) Å). Additionally, the Si–$Bi_1$–Si bond angle in ($[\mathbf{3}K(thf)_2]_2$) (90.27(4)°) is larger than in **1a** and **1b** (∼79°) and **2** (86.25(8)°). In line with that, the carborane backbone in ($[\mathbf{3}K(thf)_2]_2$) features a C⋯C distance of 2.576 Å, notably longer than that in **2** (2.268 Å), indicating a further reduced carborane cage. Furthermore, the Si–C distances in ($[\mathbf{3}K(thf)_2]_2$) (1.786(5) and 1.789(5) Å) are significantly shorter than those in **1a** and **1b** (1.923(2)–1.937(4) Å) and in **2** (1.851(8) Å). These structural features confirm that the open cage in ($[\mathbf{3}K(thf)_2]_2$) corresponds to a *nido*-carborane anion. It should be mentioned that complex **2** can also be synthesized *via* a metathesis reaction between **1b** and ($[\mathbf{3}K(thf)_2]_2$) in THF at room temperature. In addition, complex ($[\mathbf{3}K(thf)_2]_2$) can be obtained through the one-electron

Open Access Article. Published on 19 May 2025. Downloaded on 6/2/2025 5:20:26 PM.
This article is licensed under a Creative Commons Attribution 3.0 Unported Licence.

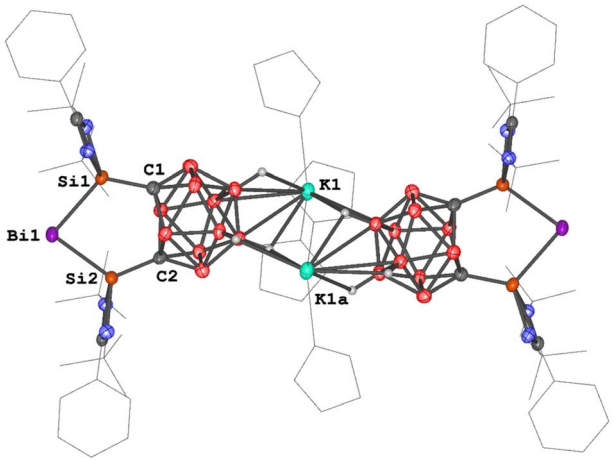


Fig. 5 Molecular structure of ([3K(thf)$_2$]$_2$). Thermal ellipsoids are drawn at the 50% probability level. H atoms and solvent molecules are omitted for clarity. Selected bond lengths (Å) and angles (deg.): Bi$_1$–Si$_1$ 2.6266(13), Bi$_1$–Si$_2$ 2.6138(13), C$_1$···C$_2$ 2.576, Si$_1$–C$_1$ 1.786(5), Si$_2$–C$_2$ 1.789(5), Si$_2$–Bi$_1$–Si$_1$ 90.27(4), C$_1$–Si$_1$–Bi$_1$ 116.52(16), C$_2$–Si$_2$–Bi$_1$ 115.93(16).

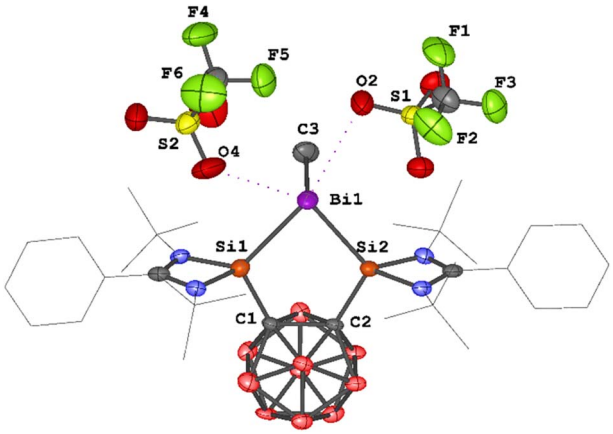


Fig. 6 Molecular structure of **4**. Thermal ellipsoids are drawn at the 50% probability level. H atoms and solvent molecules are omitted for clarity. Selected bond lengths (Å) and angles (deg.): Bi$_1$–Si$_2$ 2.7003(17), Bi$_1$–Si$_1$ 2.7160(19), Bi$_1$–C$_3$ 2.278(9), C$_2$–C$_1$ 1.717(9), Si$_1$–C$_1$ 1.929(7), Si$_2$–C$_2$ 1.917(6), Si$_1$–Bi$_1$–Si$_2$ 80.44(5), C$_1$–Si$_1$–Bi$_1$ 112.1(2), C$_2$–Si$_2$–Bi$_1$ 112.24(19), C$_3$–Bi$_1$–Si$_1$ 96.5(2), C$_3$–Bi$_1$–Si$_2$ 94.7(3).

reduction of complex **2** with $KC_8$ in THF (Scheme 2). This indirectly confirms the redox reversibility between the family members of this Bi$^{I}$ series.

The reactivity of **1b** towards methyl trifluoromethanesulfonate (MeOTf) was also investigated to evaluate the nucleophilic character of Bi$^{I}$. Upon addition of MeOTf at 40 °C in DCM, the yellow solution of **1b** gradually decolorized over 4 hours, yielding colorless {[Si$^{II}$(*closo*-CB)Si$^{II}$]BiMe} [OTf]$_2$ (**4**) in 61% yield after workup (Scheme 3). The $^{1}$H NMR spectrum of **4** in DCM-$d_2$ displays a singlet at $\delta = 2.47$ ppm for the methyl group,[37] downfield-shifted compared to free $BiMe_3$ ($\delta = 1.11$ ppm).[37a] The $^{29}$Si{$^{1}$H} NMR spectrum exhibits a singlet at $\delta =$ 62.0 ppm, significantly upfield-shifted compared to **1a** ($\delta = 68.7$ ppm) and **1b** ($\delta = 66.9$ ppm) but downfield-shifted relative to ([3K(thf)$_2$]$_2$) ($\delta = 51.8$ ppm). The $^{19}$F NMR spectrum shows a singlet at $\delta = -78.7$ ppm. Notably, treatment of **4** with $PMe_3$ in DCM at room temperature quantitatively regenerated **1b** immediately along with the formation of $PMe_4OTf$.

An scXRD analysis revealed that **4** crystallizes in the monoclinic space group $P2_1/n$. The dication in **4** features a five-membered $C_2Si_2Bi$ ring, with a methyl group and two triflate anions coordinated to the bismuth atom (Fig. 6). The bismuth center thus adopts a distorted tetragonal pyramidal geometry ($\tau_5 = 0.25$),[37b] with the methyl group occupying the apical position, suggesting the presence of a lone electron pair opposite the tetragonal plane. The Si–Bi bond lengths in **4** (2.7003(17) and 2.7160(19) Å) are significantly longer than those observed in complexes **1–3** (**1**: 2.5774(6)–2.5958(9) Å; **2**: 2.576(2) Å; **3**: 2.6266(13) and 2.6138(13) Å). The Bi$_1$–C$_3$ bond length of 2.278(9) Å in **4** is comparable to that in the [BiMe]$^{2+}$ complexes derived from **II** (2.300 Å)[25] and **III** (2.247(7) Å).[26] Notably, the shortest Bi···O interaction between the bismuth center and the two triflate anions in **4** is 3.025 Å, indicating weak coordination between the bismuth center and the triflate anions.

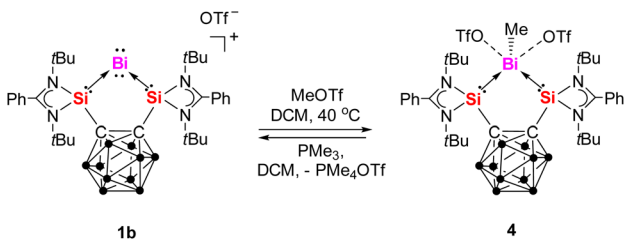


Scheme 3 Reaction of **1b** with MeOTf and the reverse reaction with $PMe_3$.

## Computational analysis

To elucidate the electronic structures of these monovalent bismuth complexes, Density Functional Theory (DFT) calculations were performed using the CAM-B3LYP/def2-TZVPD level in Gaussian 16 (see ESI† for details).[38] Table 1 compiles the HOMO–LUMO gaps of these species, confirming the predominantly single-determinant character of their wavefunctions and

Table 1 Molecular properties (ionization potential (IP), HOMO–LUMO gap (H–L gap), first hyperpolarizabilities, $\beta$, and QTAIM charges) computed for the XRD structures of **1a**, **2**, and **3** at the CAM-B3LYP/def2-TZVPD level of theory. Charges of C$_1$ and C$_2$ are considered equivalent. For more details see Fig. S31. $\beta$ values are expressed in (a.u.)

| QTAIM charges | 1a | 2 | 3 |
|---|---|---|---|
| Bi | 0.10 | −0.31 | −0.45 |
| C | −1.75 | −2.28 | −2.54 |
| BH cage | 1.98 | 2.28 | 1.99 |
| IP (eV) | 9.10[a] | 4.59 | 2.58 |
| H–L gap (eV) | 6.02[a] | 4.23 | 3.15 |
| $\beta$ (a.u.) | $8.40 \times 10^{2}$[a] | $2.74 \times 10^{3}$ | $7.18 \times 10^{3}$ |

[a] Values computed without considering the iodide counterion to permit a direct comparison among the species.


© 2025 The Author(s). Published by the Royal Society of Chemistry

Open Access Article. Published on 19 May 2025. Downloaded on 6/2/2025 5:20:26 PM.
This article is licensed under a Creative Commons Attribution 3.0 Unported Licence.

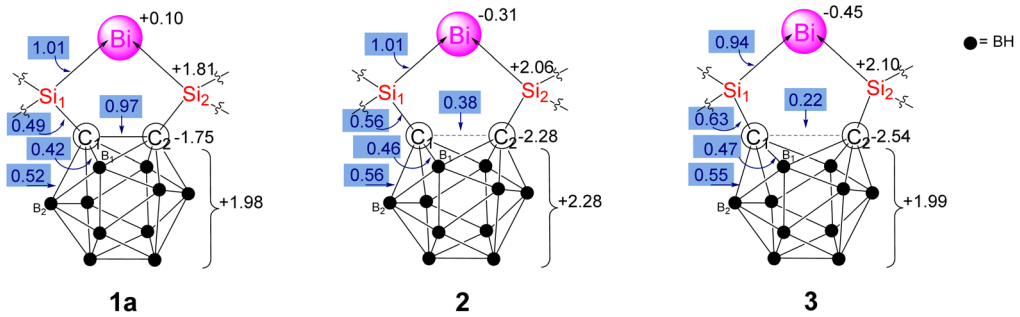


Fig. 7 Evolution of selected QTAIM atomic charges (in black) and delocalization indices (shaded and blue) of **1a**, **2** and **3** structures upon reduction.

thus supporting the use of Kohn–Sham DFT as an appropriate method. Moreover, to discard large electron delocalization errors, we have compared CAM-B3LYP and B3LYP values, the latter of which are included in the ESI for comparison (see ESI, Table S11 and Fig. S34†). The experimental scXRD data were used for the analysis, although several optimized structures—which show good agreement with the experimental ones—are also included in the ESI for comparison (see Fig. S35 and S36†). Table 1 includes the ionization potential of these species, which serves as an indication of their stability with respect to the loss of one electron, and the first hyperpolarizabilities, $\beta$. The first hyperpolarizability increases from **1a** to **2**, and **2** to **3**, reaching relatively large values which are compatible with delocalized charge distributions. In order to assess the changes in the electron distribution upon reduction, we have also employed the quantum theory of atoms in molecules (QTAIM)[39] partition to compute atomic charges and delocalization indices (DI), which are covalent bond orders.[40,41] We also run various tests to discard the electride character of **2** and **3**.[42,43] We carried out a complete topological analysis of the electron density for **1a**, **2**, and **3**, identified the critical points according to QTAIM, and examined the regions with negative values of the Laplacian of the electron density. No features indicative of an isolated electron—such as a non-nuclear attractor or regions of localized electron density revealed by Laplacian analysis, which are characteristic of electrides—were identified (see Section D4 in the ESI†). Conversely, the first hyperpolarizabilities of these compounds (see Table 1) are consistent with the presence of labile and loosely bound electrons, albeit not isolated or localized as expected in electrides.

The skeleton of **1a**, **2**, and **3** is divided into four parts: the Bi center, the two amidinato silylene units, and the carborane cage. The amidinato silylene units barely change upon reduction from **1a** to **2**, and **2** to **3**, and their data is only included in

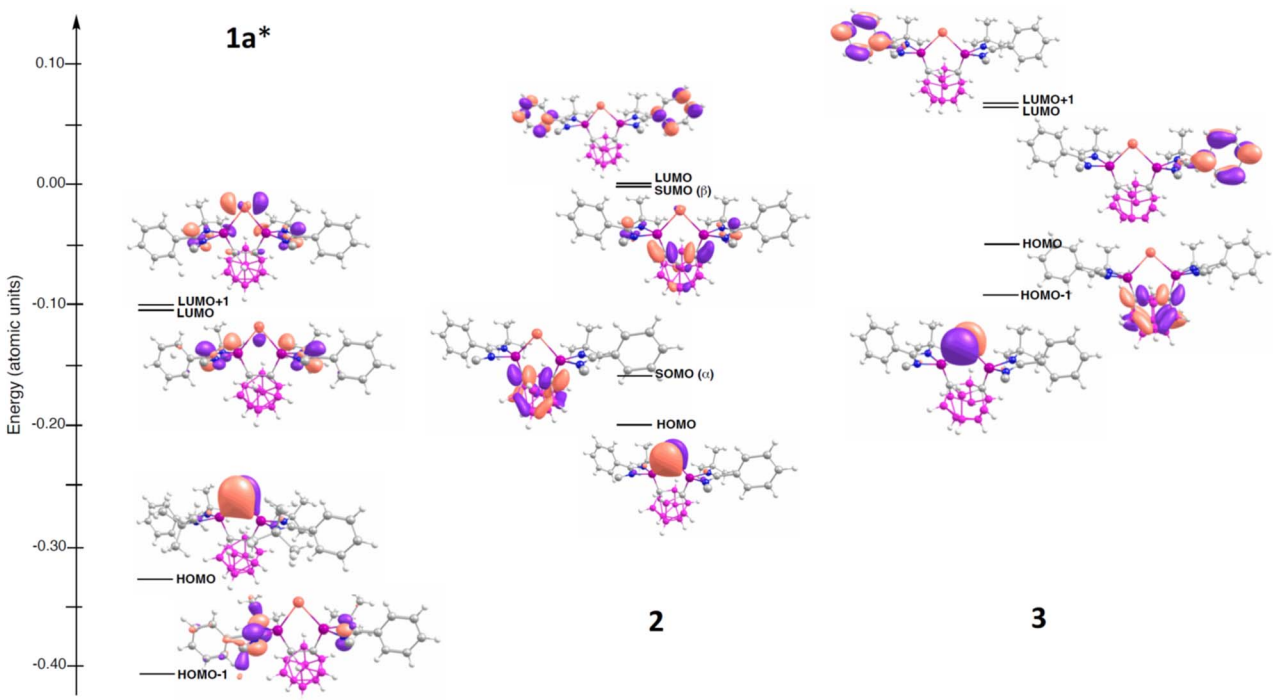


Fig. 8 Molecular orbital diagrams for selected orbitals of complexes **1a** (*without considering the $I^-$ counterion), **2**, and **3**. The front *tert*-butyl groups of the silylenyl units are removed for clarity. Molecular orbitals isovalue of 0.050 e Å–3.

© 2025 The Author(s). Published by the Royal Society of Chemistry

Open Access Article. Published on 19 May 2025. Downloaded on 6/2/2025 5:20:26 PM. This article is licensed under a Creative Commons Attribution 3.0 Unported Licence.

the ESI† for the sake of completion. Fig. 7 and Table 1 contain data concerning the electron distribution of the relevant parts of structures **1a**, **2**, and **3**.

We focus on the Bi center, the two carbon atoms in the carborane cage, and the rest of the cage (BH cage, hereafter). **1a** exhibits a regular 2c–2e bond (DI = 1.01) between Bi and Si (which is essentially maintained after reduction to **2** and **3**), while the bonds between Si and the C atoms in the carborane cage are partially covalent (DI = 0.49) with a high ionic component (Si holds a +2.06 charge, whereas C has a large negative charge of −1.75*e*). **1a** also exhibits a C–C covalent bond (DI = 0.97) within the carborane cage.

Upon reduction of **1a** to **2**, the most significant change is the reduction of the C–C bonding interaction (DI = 0.38), which further decreases upon reduction to **3** (DI = 0.22). This C–C weakening is caused by the opening of the cage at the top, as reflected in the increase of the C–C bond distance from 1.69 Å in **1a** to 2.27 Å in **2**, and subsequently to 2.58 Å in **3**. The cage opening is accompanied by a slight increase of the covalent bond orders between C and the neighboring B atoms (see ESI, Fig. S31†), and a slight increase of the Si–C bond strength, which is reflected by the higher covalent character (DI = 0.56 in **2**, DI = 0.63 in **3**). This electron reorganization is also reflected in the picture of the Laplacian of the electron density given in Fig. S32 and S33,† and the number of electrons localized in the C atoms (see ESI, Fig. S31†).

Hence, upon reduction from **1a** to **2**, the extra electron mostly localizes in the carborane cage, especially in the carbon atoms, as the BH cage actually loses some electron density upon reduction. The Bi atomic charge also increases by 0.4*e*. Based on the calculated partial charge distribution, resonance structure **2′** (Scheme 2) is proposed for compound **2**, in which the negative charges are delocalized over the bismuth atom and the carborane cage, while the two positive charges are distributed over the two silicon atoms. Upon reduction from **2** to **3**, 0.26 additional electrons localize in each C atom, whereas the other half electron is split between the Bi, which has now −0.45 electrons, and the BH cage, which restores the +2 charge it had in **1a**.

The analysis of the molecular orbitals aligns well with the conclusions drawn thus far (see Fig. 8). The SOMO of the $Bi^{I}$ compound **2** shows a large fraction of the electron density of the unpaired electron on the C atoms of the carborane (Fig. 8). This stabilized σ* orbital is reminiscent of the $N^{I}$ radical {[$Si^{II}$(*closo*-CB)$Si^{II}$]$N^{I}$} supported by the same bis(silylenyl) carborane ligand[35] and the diphenyl-o-carborane system reported by Adillon *et al.*[44]

## Conclusion

In summary, we have successfully synthesized and characterized a series of bis(silylene)-stabilized monovalent single atom bismuth complexes supported by a chelating bis(silylenyl)-*o*-carborane ligand. The redox-active nature of the carborane scaffold plays a crucial role in modulating the electronic structures of these $Bi^{I}$ complexes. The one-electron reduction of the cationic complex **1b** with $KC_8$ afforded the neutral radical complex **2**, while its two-electron reduction with $KC_{10}H_8$ led to the formation of the anionic dimeric complex **3**. These transformations highlight the remarkable redox flexibility of the bis(silylenyl)carborane framework in stabilizing monovalent bismuth. Furthermore, the reversibility of the redox processes, as demonstrated by the quantitative regeneration of **1b** upon oxidation of **2** with AgOTf, underscores the dynamic redox behavior of these complexes. X-ray crystallographic analyses and spectroscopic data reveal significant structural variations among **1–3**, particularly in the Bi–Si bonding and carborane core geometry. DFT calculations revealed that upon reduction from **1a** to **2**, the added electron predominantly localizes within the carborane cage, with a marked preference for the carbon atoms. This localization weakens the central C–C bond. A similar trend is observed in the subsequent reduction from **2** to **3**, where the additional electron again accumulates in the carborane framework. Further analysis rules out the possibility that these species exhibit the characteristics of molecular electrides. Overall, this work expands the understanding of bismuth redox chemistry and the role of cooperative carborane-based silylene ligands in stabilizing low-valent main-group species. The unique electronic properties of these robust $Bi^{I}$ complexes are expected to pave the way to new types of Bi-based redox catalysts.

## Data availability

All experimental and computational data associated with this work are available in the ESI.†

## Author contributions

Jian Xu carried out the synthetic experiments and analyzed the experimental data. Shenglai Yao assisted in the XRD refinement of the compounds and edited the manuscript. Christian Lorent collected the EPR data. Verònica Postils performed the DFT calculations. Verònica Postils and Eduard Matito analyzed the electronic structure of the compounds. Matthias Driess supervised the work and edited the manuscript. The manuscript was written through the contribution of all authors.

## Conflicts of interest

There are no conflicts to declare.

## Acknowledgements

This work was funded by DFG (German Research Foundation) under Germanýs Excellence Strategy – EXC 2008-390540038 – UniSysCat and DR-226/25-1. We particularly thank Paula Nixdorf for the assistance in the XRD measurements and Christian Teutloff from the FU Berlin for helpful discussion regarding the EPR data. Grants PID2022-140666NB-C21 funded by MCIN/AEI/10.13039/501100011033 and "FEDER Una manera de hacer Europa", and the grants funded by the Gobierno Vasco (IT1584-22, and PIBA_2023_1_0055) are acknowledged. V.P. also thanks WBI (Wallonie-Bruxelles International) for her IN.WBI Excellence Grant. Calculations were performed on the computing facilities at the DIPC.


© 2025 The Author(s). Published by the Royal Society of Chemistry

Open Access Article. Published on 19 May 2025. Downloaded on 6/2/2025 5:20:26 PM. This article is licensed under a Creative Commons Attribution 3.0 Unported Licence.

## Notes and references


1 R. Mohan, *Nat. Chem.*, 2010, **2**, 336.
2 P. De Marcillac, N. Coron, G. Dambier, J. Leblanc and J. P. Moalic, *Nature*, 2003, **422**, 876–878.
3 N. Yang and H. Sun, *Coord. Chem. Rev.*, 2007, **251**, 2354–2366.
4 C. Stewart, K. Konstantinov, S. McKinnon, S. Guatelli, M. Lerch, A. Rosenfeld, M. Tehei and S. Corde, *Phys. Med.*, 2016, **32**, 1444–1452.
5 X. Huang, S. Huang, P. Biswas and R. Mishra, *J. Phys. Chem. C*, 2016, **120**, 28924–28932.
6 P. Sprenger, W. Kleist and J. D. Grunwaldt, *ACS Catal.*, 2017, **7**, 5628–5642.
7 V. K. Srivastava, M. Maiti, G. C. Basak and R. V. Jasra, *J. Chem. Sci.*, 2014, **126**, 415–427.
8 H. W. Moon and J. Cornella, *ACS Catal.*, 2022, **12**, 1382–1393.
9 M. Mato, F. Wang and J. Cornella, *Adv. Synth. Catal.*, 2024, **366**, 740–744.
10 C. Lichtenberg, *Chem. Commun.*, 2021, **57**, 4483–4495.
11 M. Mato, D. Spinnato, M. Leutzsch, H. W. Moon, E. J. Reijerse and J. Cornella, *Nat. Chem.*, 2023, **15**, 1138–1145.
12 T. Tsuruta, D. Spinnato, H. W. Moon, M. Leutzsch and J. Cornella, *J. Am. Chem. Soc.*, 2023, **145**, 25538–25544.
13 S. Ni, D. Spinnato and J. Cornella, *J. Am. Chem. Soc.*, 2024, **146**, 22140–22144.
14 P. Zhang, F. Benner, N. F. Chilton and S. Demir, *Chem*, 2022, **8**, 717–730.
15 E. R. Pugliese, F. Benner and S. Demir, *Chem.–Eur. J.*, 2023, **29**, e202302687.
16 P. Zhang, R. Nabi, J. K. Staab, N. F. Chilton and S. Demir, *J. Am. Chem. Soc.*, 2023, **145**, 9152–9163.
17 G. Frenking, M. Hermann, D. M. Andrada and N. Holzmann, *Chem. Soc. Rev.*, 2016, **45**, 1129–1144.
18 S. Yao, Y. Xiong and M. Driess, *Acc. Chem. Res.*, 2017, **50**, 2026–2037.
19 P. K. Majhi and T. Sasamori, *Chem.–Eur. J.*, 2018, **24**, 9441–9455.
20 S. Yao, Y. Xiong, A. Saddington and M. Driess, *Chem. Commun.*, 2021, **57**, 10139–10153.
21 S. Yao, A. Saddington, Y. Xiong and M. Driess, *Acc. Chem. Res.*, 2023, **56**, 475–488.
22 W. Petz and G. Frenking, *Adv. Inorg. Chem.*, 2022, **79**, 247–299.
23 R. Deb, P. Balakrishna and M. Majumdar, *Chem.–Asian J.*, 2022, **17**, e202101133.
24 M. M. Siddiqui, S. K. Sarkar, M. Nazish, M. Morganti, C. Köhler, J. Cai, L. Zhao, R. Herbst-Irmer, D. Stalke, G. Frenking and H. W. Roesky, *J. Am. Chem. Soc.*, 2021, **143**, 1301–1306.
25 X. Wang, B. Lei, Z. Zhang, M. Chen, H. Rong, H. Song, L. Zhao and Z. Mo, *Nat. Commun.*, 2023, **14**, 2968.
26 J. Xu, S. Pan, S. Yao, C. Lorent, C. Teutloff, Z. Zhang, J. Fan, A. Molino, K. B. Krause, J. Schmidt, R. Bittl, C. Limberg, L. Zhao, G. Frenking and M. Driess, *J. Am. Chem. Soc.*, 2024, **146**, 6025–6036.
27 A. Saddington, S. Yao and M. Driess, *Adv. Inorg. Chem.*, 2023, **82**, 119–156.
28 Y. P. Zhou, M. Karni, S. Yao, Y. Apeloig and M. Driess, *Angew. Chem., Int. Ed.*, 2016, **55**, 15096–15099.
29 Y. Wang, M. Karni, S. Yao, A. Kaushansky, Y. Apeloig and M. Driess, *J. Am. Chem. Soc.*, 2019, **141**, 12916–12927.
30 Y. Wang, M. Karni, S. Yao, Y. Apeloig and M. Driess, *J. Am. Chem. Soc.*, 2019, **141**, 1655–1664.
31 J. Xu, C. Dai, S. Yao, J. Zhu and M. Driess, *Angew. Chem., Int. Ed.*, 2022, **61**, e202114073.
32 J. Xu, S. Pan, S. Yao, G. Frenking and M. Driess, *Angew. Chem., Int. Ed.*, 2022, **61**, e202209442.
33 S. Yao, A. Kostenko, Y. Xiong, A. Ruzicka and M. Driess, *J. Am. Chem. Soc.*, 2020, **142**, 12608–12612.
34 S. Yao, A. Kostenko, Y. Xiong, C. Lorent, A. Ruzicka and M. Driess, *Angew. Chem., Int. Ed.*, 2021, **60**, 14864–14868.
35 S. Yao, T. Szilvási, Y. Xiong, C. Lorent, A. Ruzicka and M. Driess, *Angew. Chem., Int. Ed.*, 2020, **59**, 22043–22047.
36 Y. P. Zhou, S. Raoufmoghaddam, T. Szilvási and M. Driess, *Angew. Chem., Int. Ed.*, 2016, **55**, 12868–12872.
37 (*a*) J. Ramler, F. Fantuzzi, F. Geist, A. Hanft, H. Braunschweig, B. Engels and C. Lichtenberg, *Angew. Chem., Int. Ed.*, 2021, **60**, 24388–24394; (*b*) A. W. Addison, T. N. Rao, J. Reedijk, J. van Rijn and G. C. Verschoor, *J. Chem. Soc., Dalton Trans.*, 1984, 1349–1356.
38 M. J. Frisch, G. W. Trucks, H. B. Schlegel, G. E. Scuseria, M. A. Robb, J. R. Cheeseman, G. Scalmani, V. Barone, G. A. Petersson, H. Nakatsuji, X. Li, M. Caricato, A. V. Marenich, J. Bloino, B. G. Janesko, R. Gomperts, B. Mennucci, H. P. Hratchian, J. V. Ortiz, A. F. Izmaylov, J. L. Sonnenberg, D. Williams-Young, F. Ding, F. Lipparini, F. Egidi, J. Goings, B. Peng, A. Petrone, T. Henderson, D. Ranasinghe, V. G. Zakrzewski, J. Gao, N. Rega, G. Zheng, W. Liang, M. Hada, M. Ehara, K. Toyota, R. Fukuda, J. Hasegawa, M. Ishida, T. Nakajima, Y. Honda, O. Kitao, H. Nakai, T. Vreven, K. Throssell, J. A. Montgomery Jr, J. E. Peralta, F. Ogliaro, M. J. Bearpark, J. J. Heyd, E. N. Brothers, K. N. Kudin, V. N. Staroverov, T. A. Keith, R. Kobayashi, J. Normand, K. Raghavachari, A. P. Rendell, J. C. Burant, S. S. Iyengar, J. Tomasi, M. Cossi, J. M. Millam, M. Klene, C. Adamo, R. Cammi, J. W. Ochterski, R. L. Martin, K. Morokuma, O. Farkas, J. B. Foresman and D. J. Fox, *Gaussian 16 Rev C01*, 2016.
39 R. F. W. Bader, *Atoms in Molecules: A Quantum Theory*, Oxford University Press, Oxford, 1990.
40 X. Fradera, M. A. Austen and R. F. W. Bader, *J. Phys. Chem. A*, 1999, **103**, 304–314.
41 E. Matito, M. Solà, P. Salvador and M. Duran, *Faraday Discuss.*, 2007, **135**, 325–345.
42 V. Postils, M. Garcia-Borràs, M. Solà, J. M. Luis and E. Matito, *Chem. Commun.*, 2015, **51**, 4865–4868.
43 S. P. Sitkiewicz, E. Ramos-Cordoba, J. M. Luis and E. Matito, *J. Phys. Chem. A*, 2021, **125**, 4819–4826.
44 E. H. Adillon and J. C. Peters, *J. Am. Chem. Soc.*, 2024, **146**, 30204–30211.


© 2025 The Author(s). Published by the Royal Society of Chemistry